Journal of the European Ceramic Society **15** (1995) 1149–1156

0955-2219(95)00079-8
0955-2219/95/$9.50

Study of $Li_{1+x}Al_xTi_{2-x}(PO_4)_3$ for Li^+ Potentiometric Sensors

M. Cretin, P. Fabry & L. Abello

Laboratoire d'Ionique et d'Electrochimie du Solide de Grenoble, CNRS URA D1213, ENSEEG, B.P. 75, 38402 Saint Martin d'Heres, Cedex, France

(Received 21 January 1995; revised version received 18 May 1995; accepted 19 May 1995)

Abstract

Mineral compounds $Li_{1+x}Al_xTi_{2-x}(PO_4)_3$ (x = 0 and x = 0·3) have been made by co-grinding and soil–gel processes. Structural characterizations by X-ray diffraction and Raman spectroscopy indicate that alumina substitution (x = 0·3) does not modify the crystallographic structure, whatever the synthesis process: compounds crystallize in the rhombohedral system with an R-3C space group. The use of the sol–gel route makes low-temperature sintering (950°C) easier and, moreover, leads to ceramics with a high water stability. $Li_{1.3}Al_{0.3}Ti_{1.7}(PO_4)_3$ compounds are fast ionic conductors: $\sigma_{25°C}$ varies from 15^{-5} to 10^{-4} S cm^{-1}, depending on the synthesis process. They have been used as ionic membranes for lithium-selective electrodes. Sensors prepared with sol–gel membranes have the best performance: the detection limit is 1·4 × 10^{-4} mol dm^{-3}. The potassium and the protonic selectivity properties are attractive for such electrodes. For sodium, they need to be improved for biomedical applications.

1 Introduction

During the last few years, numerous studies on lithium ionic conductors of NASICON-type structure have been published. Because of their significant ionic conductivity, the high reduction potential and low atomic mass of lithium, these materials were destined to be used as solid electrolytes for secondary batteries.[1–5] These ionocovalent compounds, of general formula $Li_{1+x}M'x$ (III)$_{2-x}$(IV)$(PO_4)_3$, have a particular crystallographic structure: the NASICON framework consists of a 3D network of PO_4 tetrahedra sharing corners with TiO_6 octahedra and a 3D linked interstitial space occupied by Li^+ ions.[1] These materials may have good selectivity properties as membranes for ion-selective electrodes. The possibility of similar systems has already been shown with the NASICON $Na_{1+x}Zr_2Si_xP_{3-x}O_{12}$, a sodium conductor used in sodium potentiometric sensors.[6,7]

To realize crystallized membranes for lithium electrodes, we have synthesized $Li_{1+x}M'_x$(III)M_{2-x}(IV)$(PO_4)_3$ type compounds, with M' = Al and M = Ti, by different routes. First, we have chosen the most conducting compound of this group: $Li_{1.3}Al_{0.3}Ti_{1.7}(PO_4)_3$. We have also synthesized $LiTi_2(PO_4)_3$ to compare the properties of the doped (x = 0·3) and the undoped (x = 0) ceramics. We have used two processes for their preparation: co-grinding (A) and a sol–gel (B) route. Various physico-chemical characterizations have been carried out on rough and calcined powders, and sintered materials. Afterwards, the samples were used in potentiometric sensors. The results obtained with the different methods are compared.

2 Synthesis and Structural Properties

2.1 Co-grinding synthesis (method A)

Starting materials were Li_2CO_3 (Janssen®, 99% pure), Al_2CO_3 (Baikowski®, 99·99% pure), TiO_2 (Merck®, 99% pure) and $(NH_4)_2HPO_4$ (R.P.®, 99% pure). A stoichiometric mixture was ground for ~100 h with zirconia grinding balls in ethanol. The approximate ratio was 1/3 powder, 1/3 grinding balls and 1/3 ethanol. Then, it was dried and calcined for 2 h at 900°C to decompose the precursors. Afterwards the resulting material was reground.[4] For total decomposition, we had to reheat at 900°C and regrind the product. Specific area of the obtained mixture (measured by the B.E.T. method) is 1·7 m^2 g^{-1} for dried powder. The granulometry is dispersed so that the particle sizes vary from 0·5 to 2 μm (Fig. 1(a)).

The synthesized powder was pressed into pellets at a pressure of 2500 bar (250 MPa) and sintered for 2 h at 1000°C. As seen from a micrograph of a $Li_{1.3}Al_{0.3}Ti_{1.7}(PO_4)_3$ broken pellet obtained by scanning electron microscopy (SEM) (Fig. 1(b)),

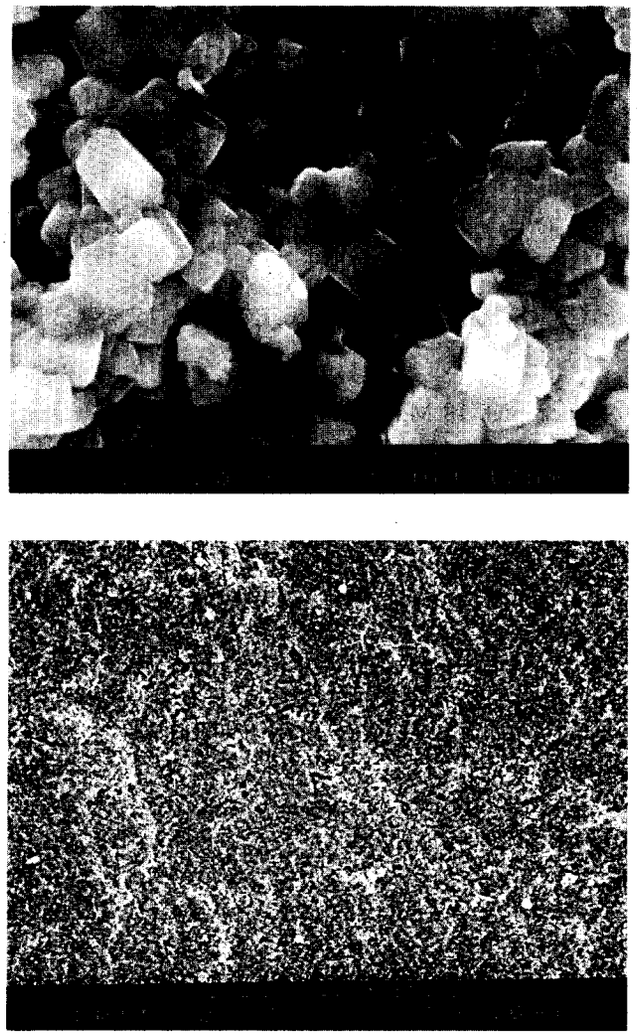

Fig. 1. Scanning electron micrographs of (a) $Li_{1\cdot3}Al_{0\cdot3}Ti_{1\cdot7}(PO_4)_3$ powder synthesized by the co-grinding process and calcined at 900°C and (b) $Li_{1\cdot3}Al_{0\cdot3}Ti_{1\cdot7}(PO_4)_3$ pellet synthesized by theco-grinding process (sintered at 1000°C).

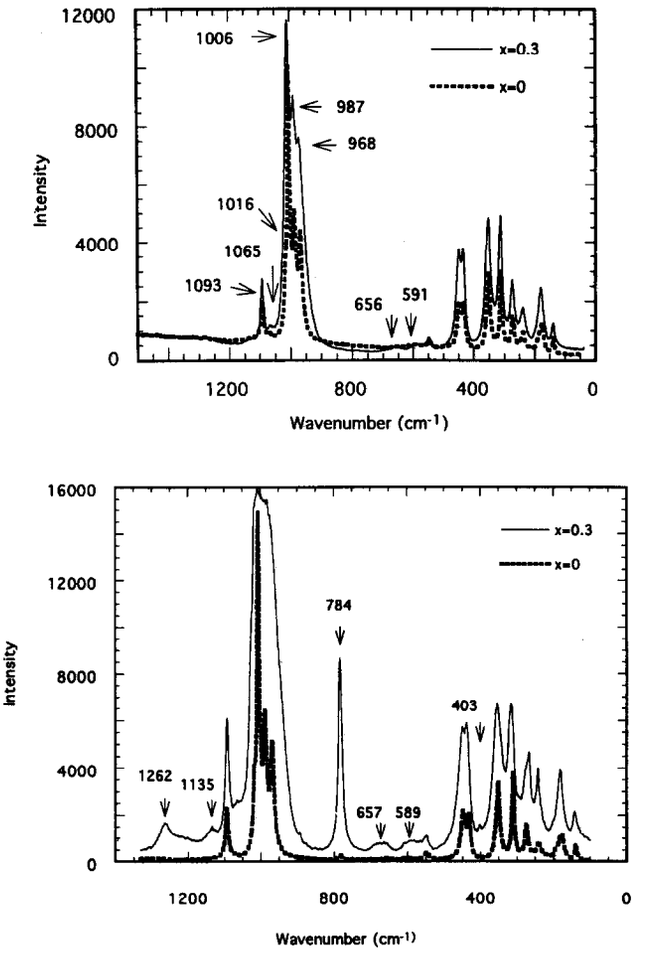

Fig. 2. Raman spectra of (a) co-ground pellet sintered at 1000°C and (b) sol–gel pellet sintered at 950°C.

the ceramic is compact with a packing density of 92%. On the other hand, the $LiTi_2(PO_4)_3$ samples are porous: packing density is about 75%. This result is in agreement with those of Aono *et al.*[4] X-ray diffraction analysis (using $K_{\alpha 1}$ Cu radiation, λ = 0·15406 nm) was conducted with a Siemens D500® $\theta/2\theta$. Doped and undoped ceramics are single-phase materials based on the $LiTi_2(PO_4)_3$ type, with a rhombohedral structure in the R-3C space group. X-ray microanalysis connected with SEM has shown heterogeneity in the composition because of the incomplete decomposition of Li_2CO_3.

To complete the structural analysis, we studied the sintered samples by Raman scattering spectroscopy. Spectra were obtained using a Dilor® *XY* multi-channel spectrometer. The excitation source was an argon-ion laser (excitation wavelength of 514·5 nm and power of 60 mW). Raman spectra of undoped $LiTi_2(PO_4)_3$ (x = 0) and doped $Li_{1\cdot3}Al_{0\cdot3}Ti_{1\cdot7}(PO_4)_3$ (x = 0·3) polycrystalline samples synthesized by co-grinding are shown in Fig. 2(a). Assignment of the different bands of the $LiTi_2(PO_4)_3$ spectra followed the works of Barj.[9,10] Table 1 compares the Raman frequencies of this material and of $NaTi_2(PO_4)_3$.[10] Concerning the co-ground compound, the vibrational frequencies of the internal modes (wavenumber > 400 cm^{-1}) of both compounds are in agreement (Table 1). The intensity inversion between ν_1 and ν_3 has been observed previously and is due to the high electrical charge of PO_4 tetrahedra.[10] For the external modes (< 400 cm^{-1}), the assignment is delicate because of the possibility of frequency coupling between the different ions. Consequently the lithium signature, which should appear at about 300 cm^{-1}, has never been identified. In this range, the correlation with $NaTi_2(PO_4)_3$ is more difficult. For the substituted compound (x = 0·3), the intensities of the unknown bands at 656 and 591 cm^{-1} increase slightly (Fig. 2(a)). This alumina doping also induces a significant modification of the relative intensities of the bands at 1006, 987 and 968 cm^{-1}, and a general enlargement of the spectrum which is due to distortion of the $(Ti/Al)O_6$ octahedra and the PO_4 tetrahedra. Doped and undoped materials are homogeneous: Raman spectra on different areas of the pellets are identical. Li_2CO_3, identified by X-ray microanalysis, did not appear in the spectra.

Table 1. Comparison between the Raman frequencies of the different compounds

$LiTi_2(PO_4)_3$ Raman wavenumber (cm^{-1})		$NaTi_2(PO_4)_3$ Raman wavenumber (cm^{-1}) (Ref. 10)	
Co-ground (Fig. 2(a))	*Sol–gel (Fig. 2(b))*		
1093	1093	1098	$\nu 3$: $A_{1g} + 3E_g$
1065	1065	1070	(antisymmetric
1016	1016	1037	stretching vibration)
1006	1006	1009	
987	987	985	ν_1:$A_{1g}+E_g$
968	968	970	(symmetric stretching vibration)
	784		
656 and 591	657 and 589		
547	548	547	ν_4:$A_{1g} + 3E_g$
		525	(anti symmetric bending vibration)
		455	ν_2:$2A_{1g} + 2E_g$
448	448	440	(symmetric bending vibration)
432	431	432	
		418	
		382	
352	352	350	(Ti–O) vibration mode
		337	
310	310	305	vibration
274	274	273	and
239	240	255	translation
195	195	222	of
177	177	195	phosphorus ions
139	139	155	T^1 and R^1 (PO_4)
		67 and 42	vibration mode of N_a^+

2.2 Sol–gel synthesis (method B)

$LiTi_2(PO_4)_3$ and $Li_{1.3}Al_{0.3}Ti_{1.7}(PO_4)_3$ have already been successfully prepared by this process. Tohge *et al.*[11] used organic precursors for lithium and titanium: $LiOC_2H_5$ and $Ti(OC_4H_9)_4$. They also tested different sources of phosphorus: $PO(OC_2H_5)_3$ and H_3PO_4. It was shown that the use of $PO(OC_2H_5)_3$ leads to a heterogeneous gel and to a material containing TiO_2 after calcination. On the other hand, Ando *et al.*[12] synthesized the above ceramics from CH_3COOLi, $Ti(OC_4H_9)_4$, H_3PO_4, $AlCl_3.6H_2O$ and CH_3COONH_4. The use of CH_3COONH_4 gave a single-phase material without TiO_2 because acetate anions replace the OR groups and form a stable titanium–acetate complex.[13]

The precursors that we chose are $Ti(OC_4H_9)_4$ (Janssen®, 99% pure) and $Al(OC_4H_9)_3$ Janssen®, 97% pure), $NH_4H_2PO_4$ (Fluka®, >99% pure) and CH_3COOLi (Schuchardt®, 98% pure). We avoided the use of chloride precursors, because Cl_2 is generally difficult to eliminate during the sintering. We also tested other starting materials for Li precursors: $LiNO_3$ and LiOH. The pellets obtained were single-phase type $LiTi_2(PO_4)_3$, but the samples had very poor ionic conductivity, almost certainly because of lack of a part of the lithium due to Li_2CO_3, formation[14] and $LiNO_3$ departure during the drying stage. Consequently, we stopped using these type of precursors and chose CH_3COOLi.

The different stages of our sol–gel process are:

- a C_2H_5OH solution of $Ti(OC_4H_9)_4$ and $Al(OC_4H_9)_3$ is heated for 1 h at 70°C;
- an aqueous solution of CH_3COOLi and $NH_4H_2PO_4$ at 70°C is added to the first mixture;
- an excess of H_2O (70°C) (more than the stoichiometric amount required for hydrolysis of the alkoxides) is also used.

As soon as the solutions are mixed, a fine powder forms immediately. Strong stirring is used for 2 h at 70°C.

Then, the drying stage is conducted at low temperature. To facilitate the sublimation process, the product is frozen at –40°C with a Christ Alpha 2-4® freeze dryer. With this technique, the initial morphology of the powder is preserved, contrary to the usual hot or room temperature drying processes such as evaporation, centrifugation with acetone[15] or azeotropic distillation,[16] which can induce powder agglomeration. The specific area of this xerogel powder dried with our process is 52 $m^2\ g^{-1}$ and the particle size is about 0·25 μm diameter.

During a temperature analysis of the sol–gel pellets, very high shrinkage took place between 200 and 450°C (Fig. 3). In this range of temperature, differential scanning calorimetry (DSC) and thermogravimetric analysis (TGA) (Fig. 4) of the sol–gel compounds show exothermic peaks and considerable weight loss. All these phenomena are

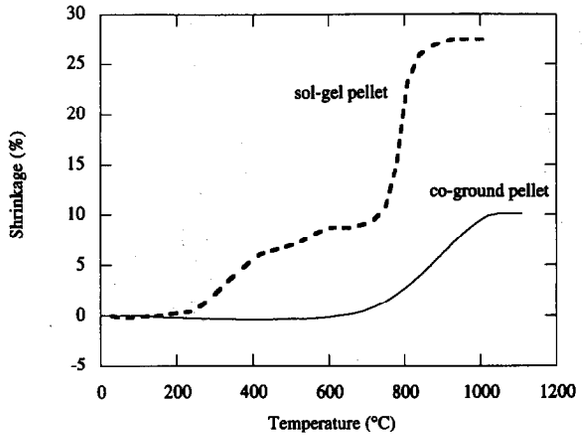

Fig. 3. Shrinkage study during the sintering of $Li_{1.3}Al_{0.3}Ti_{1.7}(PO_4)_3$ synthesized by the co-grinding and sol–gel processes.

due to the combustion of organic groups. As a consequence, to facilitate sintering, it is better to burn off the organic groups. So the powder was calcined at 550°C for 4 h. It remained amorphous according to X-ray diffraction and Raman spectroscopy but the specific area decreased (35 m^2 g^{-1}) due to low temperature sintering of the gel. Nevertheless, the particles are finer than those synthesized by the co-grinding process (Fig. 5).

Sintering is much faster for the sol–gel compounds and moreover takes place at a temperature 100°C lower than that for co-ground compounds (Fig. 3). These properties are required for very high densification. They are due to the very good reactivity of the sol–gel powder, because of its homogeneity and narrow granulometry. Subsequently, doped pellets sintered at 950°C have a packing density of about 93%. At about 640°C, compounds start to crystallize as evidenced by an exothermic peak on the DSC trace (Fig. 4). Pellets sintered at 950°C for about 2 h are mono-phase $LiTi_2(PO_4)_3$.

Raman spectra of $LiTi_2(PO_4)_3$ synthesized by both processes are in agreement (Figs 2(a) and 2(b) and Table 1), except for the presence of a

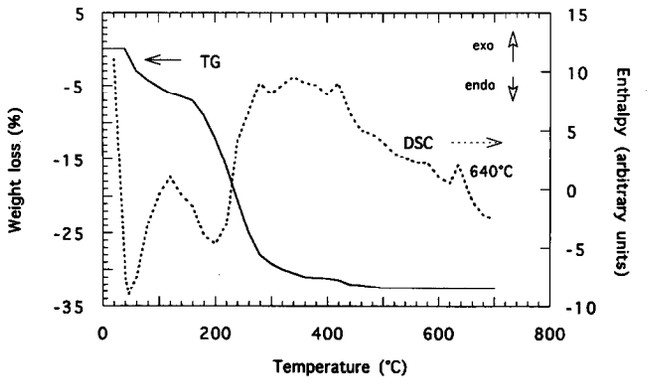

Fig. 4. Thermogravimetric and differential scanning calorimetry analysis of a doped powder synthesized by the sol–gel route.

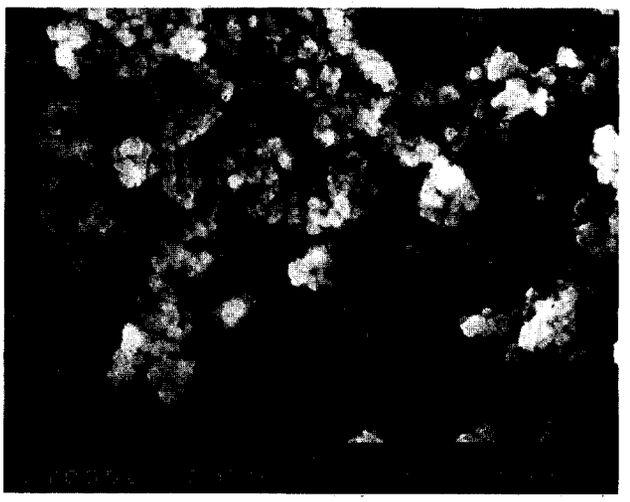

Fig. 5. Scanning electron micrograph of a $Li_{1.3}Al_{0.3}Ti_{1.7}(PO_4)_3$ powder synthesized by the sol–gel process and calcined at 550°C.

very weak band at 784 cm^{-1} on the sol–gel sample spectra. The general spectrum modifications due to the substitution do not depend on the synthesis process: for x = 0·3, we notice for both compounds the relative intensity modifications of the ν_3 and ν_1 bands and a general enlargement of the spectrum. We note the presence of new bands at 1262, 1135 and 403 cm^{-1} on the sol–gel doped material (Fig. 2(b)). Analysis of different samples and powders of $Li_{1.3}Al_{0.3}Ti_{1.7}(PO_4)_3$ have shown that intensity of the bands at 784 and 403 cm^{-1} is a function of the sample and of the analysis area, whereas the relative intensities of the other bands are constant. Consequently, the sol–gel samples contain a small amount of a second phase. This phase seems to be more important for the doped material and it is difficult to know its nature because it is invisible to X-ray diffraction. The complete assignments of the Raman spectra bands for $LiTi_2(PO_4)_3$ and $Li_{1.3}Al_{0.3}Ti_{1.7}(PO_4)_3$ are the subject of current work.

3 Physico-chemical Properties Study

3.1 Ionic conductivity

Ionic conductivity has been measured by the AC impedance method in the range 5 to 13 MHz (impedance analyser HP 4192A®). The measurements were made in a vaccum cell between 25 and 200°C, using gold evaporation electrodes. The utilization of Au blocking electrodes allows a correct separation between the bulk and electrode impedances. An example is given in Fig. 6. The respective contributions of the grains and the grain boundaries have not been separated because their characteristic frequencies are close. As a consequence, Table 2 gives the total conductivity at

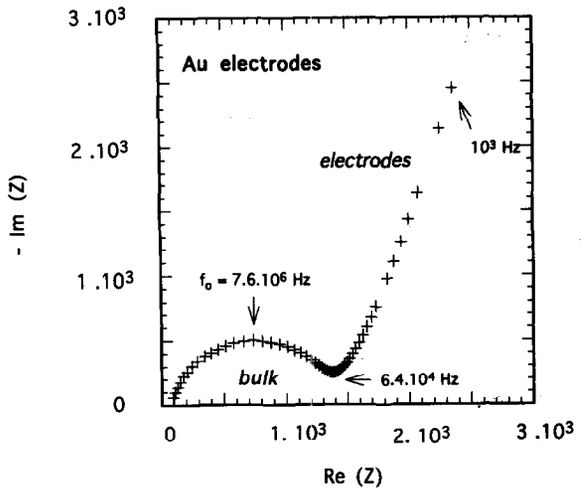

Fig. 6. Example of impedance diagram obtained at 130°C on a $Li_{1.3}Al_{0.3}Ti_{1.7}(PO_4)_3$ pellet synthesized by the sol–gel process using Au electrodes.

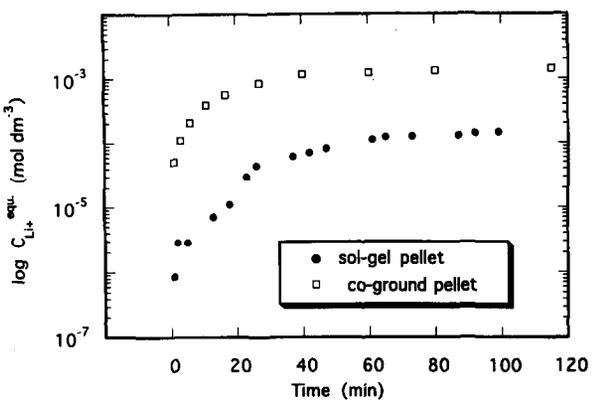

Fig. 7. Evolution of the lithium concentration in solution as a function of time for $Li_{1.3}Al_{0.3}Ti_{1.7}(PO_4)_3$ sintered pellets.

25°C and the activation energy of the different sintered samples, extracted from the Arrhenius plots.

For $x = 0$, the co-ground compound (75% packing density) and the sol–gel compound (82% packing density) are poor ionic conductors. Moreover, the sol–gel material has a high activation energy. On the other hand, $Li_{1.3}Al_{0.3}Ti_{1.7}(PO_4)_3$ ceramics have good electrical properties: very high lithium conductivity and low activation energy. These properties are better for the co-ground samples (95% packing density). The lithium conductivity enhancement for doped materials can be explained by the fact that conductivity depends on different factors:

- the carrier concentration — partial substitution of Ti (IV) by Al (III) has required lithium enhancement to maintain electroneutrality of the compound. This doping has been corroborated by the value of the lithium concentration in the ceramic, which was measured by the analysis laboratory of the CNRS (Vernaison, France);
- the carrier mobility — the octahedral substitution $(Ti/Al)O_6$ has led to a distortion of the structure, confirmed by Raman spectroscopy. Consequently, like in NASICON compounds, carrier diffusion is facilitated by structural transformation,[17] because of the slight decrease of the size of the conduction sites;
- the packing density of the sample — Aono *et al.*[4] have shown that the partial substitution of the Ti^{4+} site with Al^{3+} was very effective for enhancement of the conductivity, mainly because of the densification of the sintered pellets.

3.2 Stability in water

To determine the stability in water of the ceramics, we have recorded the lithium loss from the pellet to the solution. Samples were immersed in distilled water and the lithium concentration was measured every 10 min using a Varian AA1275BD® atomic absorption spectrometer (Fig. 7). Results in function of time are given in Fig. 7.

The values tend to a constant, with stability being achieved after about 40 min for the co-ground pellet and 60 min for the sol–gel pellet. The lithium concentration equilibrum value is $1{\cdot}4\ 10^{-3}$ mol dm^{-3} for the co-ground ceramic. We can think that the lithium concentration corresponds to equilibrum phenomena (solubility, ionic exchange, etc.). After about 100 h of immersion, we recorded 5% weight loss for this pellet. This very poor stability in water is due to the preferential solubility of parasite phases, invisible by X-ray diffraction. Li_2CO_3, identified by X-ray microanalysis, is certainly the origin of this solubility. On the other hand, sol–gel ceramics have a better stability: the equilibrum value is low, $1{\cdot}5 \times 10^{-4}$ mol dm^{-3}. In this case, weight loss is about 0·9%.

Table 2. Conductivity at 25°C and activation energy (E_a) of sintered pellets

	$LiTi_2(PO_4)_3$ ($x = 0$)				*$Li_{1.3}Al_{0.3}Ti_{1.7}(PO_4)_3$ ($x = 0{\cdot}3$)*			
	Co-ground		*Sol–gel*		*Co-ground*		*Sol–gel*	
$\sigma_{25°C}$ ($S\ cm^{-1}$)	2×10^{-6} Ref. 4	7×10^{-7}	$2{\cdot}4 \times 10^{-8}$ Ref. 12	4×10^{-8}	7×10^{-4} Ref. 4	9×10^{-5}	$3{\cdot}2 \times 10^{-4}$ Ref. 12	10^{-5}
E_a(EV)	0·37		0·51		0·37		0·40	

4 Utilization of Ceramics as Ionic Membranes in Potentiometric Sensors

The development of lithium-selective potentiometric electrodes for the determination of Li^+ activity in biological systems has already been realized, especially when using polymeric membranes.[18–23] However, the lifetime of this type of electrode is short; moreover polymers are not suitable for sterilization. Consequently, it is attractive to use ceramic membranes in potentiometric sensors for such applications. Experimentally, the specific electrode is made with the ionic ceramic, stuck at the extremity of the electrode isolant body. Inside, a silver wire covered with a silver chloride layer and immersed in lithium salt solution constitute the internal reference. Tested membranes are $Li_{1\cdot3}Al_{0\cdot3}Ti_{1\cdot7}(PO_4)_3$ synthesized by co-grinding and sol–gel processes, because of their high ionic conductivity.

The electrochemical cell is:

Ag–AgCl/Lithium salt/Ionic conductor/Analyzed solution//Saturated Calomel Electrode (SCE)

When lithium activity in the internal reference is constant, the cell potential obeys the Nernst equation:

$$E=E^0+2\cdot3RT/F \log a_{Li^+}$$

where E^0 is a constant depending on the internal (Ag–AgCl) and external (SCE) references, and consequently on temperature. R and F are the usual constants, T the absolute temperature and a_{Li^+} the lithium activity in the analysed solution. For measurements, we use generally a supported electrolyte and we have made the approximation that the ionic strength is a constant. So, as a first approximation, a_{Li^+} can be substituted for the concentration (activity coefficient is included in E^0).

4.1 Detection limit

Referring to the IUPAC recommendations, the detection limit (DL) is the crossing point of the Nernst asymptote ($2.3RT/F$ slope) and the horizontal line, corresponding to the insensitive range of the sensor. Figure 8 gives an example of a calibration curve. We used a $BaCl_2$ 10^{-1} mol dm^{-3} solution to keep constant ionic strength and also to decrease the analysed solution impedance (Ba^{2+} is not an interfering ion). Consequently, the experimental procedure for this operation is the following: the external reference electrode is equipped with an extension (double junction) containing $BaCl_2$ 10^{-1} mol dm^{-3}. The lithium salt contained in the internal reference is LiCl 10^{-1} mol dm^{-3} + $BaCl_2$ 10^{-1} mol dm^{-3}. Both electrodes are immersed in a $BaCl_2$ 10^{-1} mol dm^{-3} solution. The addition of LiCl solutions (10^{-3} to 1 mol dm^{-3} + $BaCl_2$ 10^{-1} mol dm^{-3}) and recording of the cell potential allow the calibration curve to be plotted (Fig. 8).

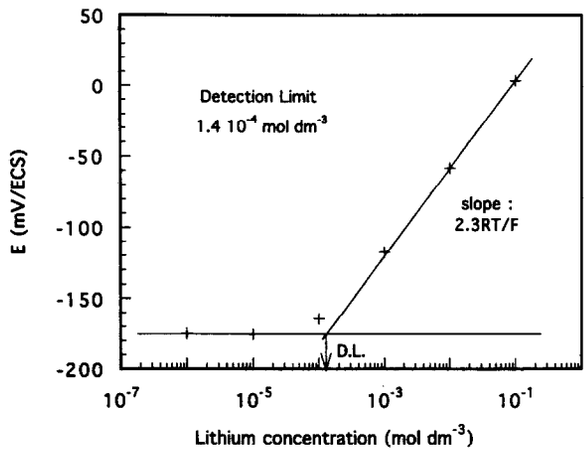

Fig. 8. Example of calibration curve and detection limit (DL) determination obtained on a Li^+ electrode using a $Li_{1\cdot3}Al_{0\cdot3}Ti_{1\cdot7}(PO_4)_3$ sol–gel membrane.

Electrodes using $Li_{1\cdot3}Al_{0\cdot3}Ti_{1\cdot7}(PO_4)_3$ membranes have a Nernst response for high lithium concentration, with a slope of $2\cdot3RT/F$ V per concentration decade. Moreover, the detection limit depends on the membrane synthesis process (Table 3): sensors using sol–gel membranes are more sensitive than those made with co-ground ones. These first type of specific electrodes are based on ionic exchanges at the membrane–solution interface. Consequently, the cell potential is a function of the ionic equilibrum at this interface. As we have seen before (stability in water), part of the lithium contained in the ceramic leaves the membrane for the solution. As a consequence, lithium concentration is more important at the interface than into the analysed solution. The detection limit of both types of sensor and the lithium solubility equilibrium value for each membrane (from Fig. 7) are compared in Table 3. The sensor sensibility is linked to the stability in water of the ceramics. Accordingly, the lithium solubility of the material is the principal limiting factor for lithium analysis with the first kind of electrodes using $Li_{1\cdot3}Al_{0\cdot3}Ti_{1\cdot7}(PO_4)_3$ ceramics. For biological appli-

Table 3. Comparison of the sensor sensibility with the concentration of Li^+ in water after about 1 h of use for co-ground and sol–gel membranes

	Co-ground membrane	*Sol–gel membrane*
Detection limit of sensors (mol dm^{-3})	$1\cdot6 \times 10^{-3}$	$1\cdot4 \times 10^{-4}$
Lithium equilibrium in water (mol dm^{-3})	$1\cdot4 \times 10^{-3}$	$1\cdot5 \times 10^{-4}$

cations, where lithium measurements in the range from 10^{-4} to 5×10^{-3} mol dm^{-3} are required,[24] sensors using co-ground membranes are not sensitive enough (DL = $1{\cdot}6 \times 10^{-3}$ mol dm^{-3}), whereas those made with sol–gel ones are usable because of their higher sensibility (DL = $1{\cdot}4 \times 10^{-4}$ mol dm^{-3}).

4.2 Ionic selectivity

The selectivity for ionic electrodes is the ability to recognize one ion amongst others. It is never perfect, because interfering ions can disturb ionic exchange at the interface. The electrode responds to the empirical Nickolskii relation:

$$E = E^{o} + 2{\cdot}3RT/z_iF \log (a_i + K_{i,j}^{pot} a_j^{zi/zj})$$

where i is the primary ion, j an interfering ion and $K_{i,j}^{pot}$ the potentiometric ion-selectivity coefficient for ion j. An example of the potentiometric ion-selectivity coefficient determination for a_{Li^+} = constant is given in Fig. 9. There are two asymptotes:

(1) $$\text{for } a_j \to 0$$
$$E^* = E^{o} + 2{\cdot}3RT/z_iF \log a_i$$

(2) $$\text{for } K_{i,j}^{pot} a_j^{zi/zj} >> a_i$$
$$E' = E^{o} + 2{\cdot}3RT/z_iF \log K_{i,j}^{pot} a_j^{zi/zj}$$

At the crossing point (Fig. 9) of both asymptotes: $K_{ij}^{pot} = a_i/(a_j^{*zi/zj})$. For the $a_j^{*zi/zj}$ value, the variation between the curve and the intersection point is 18 mV at 25°C. a_j^* is generally determined with this 18 mV variation because of the difficulty in defining the Nernst asymptote (Fig. 9).

To determine the sodium and potassium ion-selectivity coefficients, we made successive additions of a solution containing the interfering ion (LiCl 10^{-2} mol dm^{-3} + $BaCl_2$ 10^{-1} mol dm^{-3} + NaCl or KCl 10^{-1} mol dm^{-3}) in a solution of LiCl 10^{-2} mol dm^{-3} + $BaCl_2$ 10^{-1} mol dm^{-3}. To determine the protonic influence, we changed the pH of the solution by chloride acid addition. Recording and plotting of the cell potential as a function of the interfering ion lead to a_j^* determination and to $K_{i,j}^{pot}$ calculation.

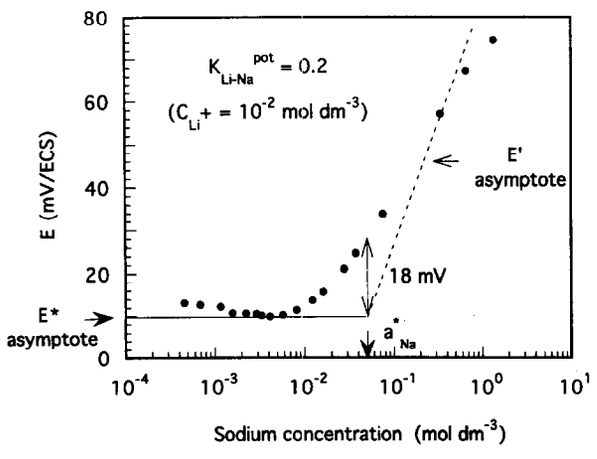

Fig. 9. Example of the determination of K_{Li-Na}^{pot} of a Li^+ electrode using a $Li_{1{\cdot}3}Al_{0{\cdot}3}Ti_{1{\cdot}7}(PO_4)_3$ co-ground membrane.

Table 4. Principal potentiometric ionic-selectivity coefficients

	Co-ground membrane	*Sol–gel membrane*
K_{Li-Na}^{pot}	0·5–1	0·2
$K_{Li\ K}^{pot}$	3×10^{-2}	5×10^{-2}
K_{Li-H}^{pot}	0·2–2	2

The synthesis process does not have a great influence on the principal potentiometric ionic-selectivity coefficients (Table 4). Both types of electrode are more selective to potassium than to sodium. This result is in agreement with Fabry and Siebert's assumption[25] that selectivity depends on the size of the interfering ion (ionic radii of Li^+, Na^+ and K^+ in 6 coordinance are 0·76, 1·02 and 1·38 Å, respectively.[8] We can explain this property by the particular structure of NASICON-type ceramics: there are two types of conduction site in the network. The way between different sites is achieved through bottlenecks, the size of which is adjustable: lattice constants depend on the stoichiometry and the composition of the material.[5] In the composition $Li_{1{\cdot}3}Al_{0{\cdot}3}Ti_{1{\cdot}7}(PO_4)_3$ the sodium mobility in the membrane is high, because the opening of the bottlenecks is sufficiently large [as a comparison, the optimal value for Na^+ diffusion is obtained for $Na_3Zr_2Si_2P_2O_{12}$ for which lattice parameters are approximately a = 9·05 Å, c = 22·9 Å (Refs. 15,16)]. As a consequence, the interface equilibrum is etablished with the contribution of the sodium contained in the analysed solution. On the other hand, the potassium is too large for the bottlenecks and then the K^+ contribution decreases greatly.

Concerning the pH effect on the sensor response, it is not due to a structural ionic exchange but arises from ionic (H^+ or OH^-) adsorption at the surface of the membrane.[26] Then, for very high protonic concentration, the electrode operates like a glass one. We note that the values of the protonic potentiometric coefficient (Table 4) are lower than those obtained with the Na^+ NASICON used in sodium-selective electrodes.[15,16,25]

5 Conclusion

The use of the sol–gel process for the synthesis of $Li_{1+x}Al_xTi_{2-x}(PO_4)_3$ (x = 0·3) is fully justified. The morphology of the sol–gel powders leads to attractive sintering properties, without modification of

the structure of the sintered samples. In spite of a lower ionic conductivity than the co-ground material, the sol–gel ceramic has a better stability in water.

For aqueous analyses, ion-selective electrodes using a doped ceramic synthezised by the sol–gel process is the more attractive: the detection limit is $1{\cdot}4 \times 10^{-4}$ mol dm^{-3}. For biomedical measurements, the ion-selective electrode must be very selective for Na^+ and K^+ (low values of $K_{Li,Na}^{pot}$ and $K_{Li,K}^{pot}$) because of the important concentration of these elements in the body. Consequently, actual values of the potentiometric coefficients, especially for Na^+, are too high for lithium analysis in blood. However, the low protonic interference is very interesting for measurements in systems such as gastric juice.

Acknowledgements

This work was supported by the 'Région Rhône-Alpes' in collaboration with RADIOMETER-ANALYTICAL S.A. The authors thank particularly Mr J. J. Fombon for his assistance in this field. They would like to acknowledge the technical assistance of M. Henault and N. Rosman.

References

1. Subramanian, M.A., Subramanian, R. & Clearfield, A., Lithium ion conductors in the system $AB(IV)_2(PO_4)_3$(B = Ti, Zr and Hf). *Solid State Ionics*, **18 & 19** (1986) 562–9.
2. Lin, Z. X., Yu, H. J., Li, S. C. & Tian, S. B., Lithium ion conductors based on $LiTi_2P_3O_{12}$ compound. *Solid State Ionics*, **31** (1988) 91–4.
3. Aono, H., Sugimoto, E., Sadaoka, Y., Imanaka, N. & Adachi, G. Y., Ionic conductivity of the lithium titanium phosphate ($Li_{1+x}M_xTi_{2-x}(PO_4)_3$, M = Al, Sc, Y and La) systems. *J. Electrochem. Soc.*, **136** (1989) 590–1.
4. Aono, H., Sugimoto, E., Sadaoka, Y., Imanaka, N. & Adachi, G. Y., Ionic conductivity of solid electrolytes based on lithium titanium phosphate. *J. Electrochem. Soc.*, **137** (1990) 1023–7.
5. Aono, H., Sugimoto E., Sadaoka, Y., Imanak, N. & Adachi, G. Y., Ionic conductivity and sinterability of lithium titanium phosphate system. *Solid State Ionics*, **40/41** (1990) 38–42.
6. Engell J. & Mortensen, S., Ion sensitive measuring device. Int. Patent WO 84:01829, Radiometer (1984)
7. Fabry, P., Gros, J. P., Million-Brodaz, J. F. & Kleitz, M., NASICON, an ionic conductor for solid-state Na^+-selective electrode. *Sensors and Actuators*, **15** (1988) 33–49.
8. Shannon, R. D., Revised effective ionic radii and systematic studies of interatomic distances in halides and chalcogenides. *Acta Cryst*, **A32** (1976) 751–67.
9. Barj, M., Perthuis, H. & Colomban, Ph., Domaines d'existence, distorsions structurales et modes de vibration des ions conducteurs dans les réseaux hotes de type NASICON. *Solid State Ionics*, **11** (1983) 157–77.
10. Barj, M., Etude de la structure statique et dynamique de quelques matériaux à mobilité ionique par spectroscopie de vibration et par diffusion de neutrons. *Thesis*, University of Paris-Nord (1987).
11. Tohge, N., Zhu, J. & Minami, T., Low-temperature preparation of $LiTi_2(PO_4)_3$ by the sol–gel process. *Chemistry Express*, **5** (1990) 973–6.
12. Ando, Y., Hirose, N., Kuwano, J., Kato, M. & Otsuka, H., Preparation of lithium ion conducting solid solutions based on $LiTi_2(PO_4)_3$ by sol–gel method. *Ceram. Today — Tomorrow's Ceram.*, (1991) 2242–52.
13. Doeuff, S., Henry, M., Sanchez, C. & Livage J., Hydrolysis of titanium alkoxides:modification of the molecular precursor by acetic acid. *J. Non-Cryst. Solids*, **89** (1987) 206–16.
14. Smaihi, M., Céramiques tritigènes à base d'orthosilicate de lithium: préparation sol–gel, mobilité du lithium et relâchement du tritium. *Thesis*, University of Paris-Sud (1990).
15. Caneiro A., Fabry, P., Khireddine, H. & Siebert, E., Performance characteristics of sodium super ionic conductors prepared by the sol–gel route for sodium ion sensors. *Anal. Chem.*, **63** (1991) 2550–7.
16. Khireddine, H., Etude des performances de capteurs potentiométriques à ions sodium utilisant des membranes de NASICON. *Thesis*, INP Grenoble (1992).
17. Boilot, J. P., Collin, G. & Colomban, Ph., Relation structure–fast ion conduction in the NASICON solid solution. *J. Solid State Chem.*, **73** (1988) 160–71.
18. Kirsch, N. N. L., Funck R. J. J., Pretsch, E. & Simon, W., Ionophore für Li^+: Membranselektivität, Darstellung und Stabilitätskonstanten in Äthanol. *Helv. Chim. Acta.*, **60** (1977) 2326–33.
19. Metzger, E., Ammann, D., Asper, R. & Simon, W., Ion selective liquid membrane electrode for the assay of lithium in blood serum. *Anal Chem.*, **58** (1986) 132–5.
20. Gadzekpo, V. P. Y., Hungerford, J. M., Kadry A. M., Ibrahim, Y. A., Xie, R. Y. & Christian, G. D., Comparative study of neutral carriers in polymeric lithium ion selective electrodes. *Anal. Chem.*, **58** (1986) 1948–53.
21. Kitazawa S., Kimura, K., Yano, H. & Shono, T., Lithium-selective polymeric membrane electrodes based on dodecylmethyl-14-crown-4. *Analyst*, **110** (1985) 295–9.
22. Kimura, K., Sakamoto, H., Kitazawa, S. & Shono, T., Novel lithium-selective ionophores bearing an easily ionizable moiety. *J. Chem. Soc., Chem. Commun.*, (1985) 669–70.
23. Sugihara, H., Okada, T. & Hiratani, K., Lithium ion-selective electrodes based on 1,10-phenanthroline derivatives. *Chem. Lett.*, (1987) 2391–2.
24. Samuel, D. & Gottesfeld, Z., Le lithium, la manie dépressive et la chimie du cerveau. *Endeavour*, **32** (1973) 122–8.
25. Fabry, P. & Siebert, E., NASICON: a sensitive membrane for ion analysis. In *Chemical Sensor Technology*, ed. Yaminhi, Kodansha, Tokyo, 1992, Vol. 4, pp. 111–24.
26. Sandifer, J. R., Theory of interfacial potential differences: effects of adsorption into hydrated (gel) and non hydrated surfaces. *Anal. Chem.*, **60** (1988) 1553–62.